Research Article | Vol. 26, No. 3 | 5 Feb 2018 | OPTICS EXPRESS 3328
Optics EXPRESS

Symmetry enhanced non-reciprocal polarization rotation in a terahertz metal-graphene metasurface

ANDREA OTTOMANIELLO,[1,2,*] SIMONE ZANOTTO,[2] LORENZO BALDACCI,[2] ALESSANDRO PITANTI,[2] FEDERICA BIANCO,[2] AND ALESSANDRO TREDICUCCI[1,2,3]

[1]*Dipartimento di Fisica "E. Fermi," Università degli studi di Pisa, 56127 Pisa, Italy*
[2]*NEST, CNR - Istituto Nanoscienze and Scuola Normale Superiore, Piazza San Silvestro 12, 56127 Pisa, Italy*
[3]*Fondazione Bruno Kessler (FBK), Via Sommarive 18, 38123 Povo, Trento, Italy*
[*]*andrea.ottomaniello@df.unipi.it*

Abstract: In the present article we numerically investigated the magneto-optical behaviour of a sub-wavelength structure composed by a monolayer graphene and a metallic metasurface of optical resonators. Using this hybrid graphene-metal structure, a large increase of the non-reciprocal polarization rotation of graphene can be achieved over a broad range of terahertz frequencies. We demonstrate that the symmetry of the resonator geometry plays a key role for the performance of the system: in particular, increasing the symmetry of the resonator the non-reciprocal properties can be progressively enhanced. Moreover, the possibility to exploit the metallic metasurface as a voltage gate to vary the graphene Fermi energy allows the system working point to be tuned to the desired frequency range. Another peculiar result is the achievement of a structure able to operate both in transmission and reflection with almost the same performance, but in a different frequency range of operation. The described system is hence a sub-wavelength, tunable, multifunctional, effective non-reciprocal element in the terahertz region.

OCIS codes: (160.3918) Metamaterials; (160.3820) Magneto-optical materials; (230.2240) Faraday effect; (230.3240) Isolators.

References and links

1. A. Tredicucci and M. S. Vitiello, "Device concepts for graphene-based terahertz photonics," IEEE J. Sel. Topics Quantum Electron. **20**(1), 130–138 (2014).
2. M. Shalaby, M. Peccianti, Y. Ozturk, and R. Morandotti, "A magnetic non-reciprocal isolator for broadband terahertz operation," Nat. Commun. **4**, 1558 (2013).
3. O. Morikawa, A. Quema, S. Nashima, H. Sumikura, T. Nagashima, and M. Hangyo, "Faraday ellipticity and faraday rotation of a doped-silicon wafer studied by terahertz time-domain spectroscopy," J. Appl. Phys. **100**(3), 033105 (2006).
4. A. Shuvaev, G. Astakhov, A. Pimenov, C. Brüne, H. Buhmann, and L. Molenkamp, "Giant magneto-optical faraday effect in hgte thin films in the terahertz spectral range," Phys. Rev. Lett. **106**(10), 107404 (2011).
5. M. Shalaby, M. Peccianti, Y. Ozturk, M. Clerici, I. Al-Naib, L. Razzari, T. Ozaki, A. Mazhorova, M. Skorobogatiy, and R. Morandotti, "Terahertz faraday rotation in a magnetic liquid: High magneto-optical figure of merit and broadband operation in a ferrofluid," Appl. Phys. Lett. **100**(24), 241107 (2012).
6. A. C. Neto, F. Guinea, N. M. Peres, K. S. Novoselov, and A. K. Geim, "The electronic properties of graphene," Rev. Mod. Phys. **81**(1), 109 (2009).
7. I. Crassee, J. Levallois, A. L. Walter, M. Ostler, A. Bostwick, E. Rotenberg, T. Seyller, D. Van Der Marel, and A. B. Kuzmenko, "Giant faraday rotation in single-and multilayer graphene," Nat. Phys. **7**(1), 48–51 (2011).
8. I. Crassee, M. Orlita, M. Potemski, A. L. Walter, M. Ostler, T. Seyller, I. Gaponenko, J. Chen, and A. Kuzmenko, "Intrinsic terahertz plasmons and magnetoplasmons in large scale monolayer graphene," Nano Lett. **12**(5), 2470–2474 (2012).
9. N. Ubrig, I. Crassee, J. Levallois, I. O. Nedoliuk, F. Fromm, M. Kaiser, T. Seyller, and A. B. Kuzmenko, "Fabry-Pérot enhanced faraday rotation in graphene," Opt. Express **21**(21), 24736–24741 (2013).
10. M. Tamagnone, C. Moldovan, J.-M. Poumirol, A. B. Kuzmenko, A. M. Ionescu, J. R. Mosig, and J. Perruisseau-Carrier, "Near optimal graphene terahertz non-reciprocal isolator," Nat. Commun. **7**, 11216 (2016).

#308159 https://doi.org/10.1364/OE.26.003328
Journal © 2018 Received 4 Oct 2017; revised 21 Nov 2017; accepted 21 Nov 2017; published 31 Jan 2018

Optics EXPRESS

11. H. Da and G. Liang, "Enhanced faraday rotation in magnetophotonic crystal infiltrated with graphene," Appl. Phys. Lett. **98**(26), 261915 (2011).
12. H. Da, Q. Bao, R. Sanaei, J. Teng, K. P. Loh, F. J. Garcia-Vidal, and C.-W. Qiu, "Monolayer graphene photonic metastructures: Giant faraday rotation and nearly perfect transmission," Phys. Rev. B **88**(20), 205405 (2013).
13. A. Fallahi and J. Perruisseau-Carrier, "Manipulation of giant faraday rotation in graphene metasurfaces," Appl. Phys. Lett. **101**(23), 231605 (2012).
14. Y. Hadad, A. R. Davoyan, N. Engheta, and B. Z. Steinberg, "Extreme and quantized magneto-optics with graphene meta-atoms and metasurfaces," ACS Photonics **1**(10), 1068–1073 (2014).
15. J. Li, Y. Zhou, B. Quan, X. Pan, X. Xu, Z. Ren, F. Hu, H. Fan, M. Qi, J. Bai, L. Wang, J. Li, and C. Gu, "Graphene–metamaterial hybridization for enhanced terahertz response," Carbon **8**, 102–112 (2014).
16. S. Zanotto, C. Lange, T. Maag, A. Pitanti, V. Miseikis, C. Coletti, R. Degl'Innocenti, L. Baldacci, R. Huber, and A. Tredicucci, "Magneto-optic transmittance modulation observed in a hybrid graphene–split ring resonator terahertz metasurface," Appl. Phys. Lett. **107**(12), 121104 (2015).
17. A. Witowski, M. Orlita, R. Stepniewski, A. Wysmołek, J. Baranowski, W. Strupiński, C. Faugeras, G. Martinez, and M. Potemski, "Quasiclassical cyclotron resonance of dirac fermions in highly doped graphene," Phys. Rev. B **82**(16), 165305 (2010).
18. M. Orlita, I. Crassee, C. Faugeras, A. Kuzmenko, F. Fromm, M. Ostler, T. Seyller, G. Martinez, M. Polini, and M. Potemski, "Classical to quantum crossover of the cyclotron resonance in graphene: a study of the strength of intraband absorption," New J. Phys. **14**(9), 095008 (2012).
19. M. Naftaly and R. E. Miles, "Terahertz time-domain spectroscopy for material characterization," Proc. IEEE **95**(8), 1658–1665 (2007).
20. J. F. O'Hara, E. Smirnova, A. K. Azad, H.-T. Chen, and A. J. Taylor, "Effects of microstructure variations on macroscopic terahertz metafilm properties," Act. Passive Electron. Compon. **2007**, 49691 (2007).
21. W. J. Padilla, A. J. Taylor, C. Highstrete, M. Lee, and R. D. Averitt, "Dynamical electric and magnetic metamaterial response at terahertz frequencies," Phys. Rev. Lett. **96**(10), 107401 (2006).
22. W. Withayachumnankul and D. Abbott, "Metamaterials in the terahertz regime," IEEE Photon. J. **1**(2), 99–118 (2009).
23. M. Tamagnone, A. Fallahi, J. R. Mosig, and J. Perruisseau-Carrier, "Fundamental limits and near-optimal design of graphene modulators and non-reciprocal devices," Nat. Photon. **8**(7), 556–563 (2014).
24. A. Woessner, M. B. Lundeberg, Y. Gao, A. Principi, P. Alonso-González, M. Carrega, K. Watanabe, T. Taniguchi, G. Vignale, M. Polini, J. Hone, R. Hillenbrand, and F. H. L. Koppens, "Highly confined low-loss plasmons in graphene–boron nitride heterostructures," Nat. Mater. **14**(4), 421–425 (2015).

1. Introduction

Non-reciprocal optical devices are essential elements in photonic systems as they provide unique capabilities such as unidirectional light flow, i.e optical isolation. The physical ground for their operation is the breaking of Lorentz reciprocity, whose first and immediate consequence is non-reciprocal polarization rotation: essentially, Faraday or Kerr effect depending whether transmission or reflection is considered.

Whilst they are largely employed across almost the whole electromagnetic spectrum, in the terahertz (THz) frequency range – a spectral region rich of applications in finger-print spectroscopy, medical diagnostics, biochemical analysis and security screening [1]– the performance of non-reciprocal devices suffers from the intrinsic losses of typical non-reciprocal materials. Some demonstrations or proposals to achieve efficient THz optical isolators exploiting iron alloys [2], doped silicon [3], mercury telluride thin films [4] and ferrofluids [5] have been realized. Nevertheless, the proposed devices do not succeed to operate at frequencies above 1.5 THz due to prohibitively high absorption.

In this context, graphene is one of the most promising materials. Among its unique properties [6], the discovery of a giant Faraday rotation ($\simeq 6^\circ$) in monolayer graphene [7, 8] has received wide attention in order to devise a new prototype of non-reciprocal element with sub-wavelength dimensions. Several theoretical and experimental works have proposed or succeeded to further enhance the non-reciprocal behavior of magnetostatically biased graphene in different ways: exploiting a Fabry-Pérot cavity [9] under a monolayer graphene or a stack of poly-methyl methacrylate (PMMA)-graphene bilayers [10], developing a photonic crystal infiltrated by graphene [11, 12] or using an array of graphene metasurfaces [13, 14]. However, most of these approaches achieve the enhancement of the Faraday effect at the expense of losing the sub-

Optics EXPRESS

wavelength dimension and working in a restricted frequency range without the possibility to tune the operating frequency.

The observation that the magneto-optical response of graphene is strongly influenced by the presence of an array of split-ring resonators (SRRs) [15, 16] motivates us to investigate whether the non-reciprocal polarization rotation can be largely enhanced adopting this hybrid metasurface. Here, by full wave simulations, we show that an appropriately designed sub-wavelength structure is able to operate both in transmission and reflection and strongly amplifies the Faraday and Kerr effects, respectively. In fact, by increasing the resonator degree of symmetry, improved performances are progressively achieved, thus obtaining higher values of both transmittance (reflectance) and Faraday angle (Kerr angle). The simulated structure is also shown to operate in a broad range of frequencies (larger than 1 THz) that can be selected by a simple resizing of the resonators forming the metasurface without losing the sub-wavelength character. Finally, we also show the significative effects of the graphene Fermi energy and the refractive index of the substrate on the non-reciprocal behaviour.

2. Description of the system

Light propagation through the structure was obtained using the finite element method through a commercial software (COMSOL Multiphysics). The structure under study is shown in Fig. 1. The monolayer graphene is positioned at the top. It is simulated as a 1 nm thick layer in order to relieve the computational effort in the simulations. We checked that this setting correctly reproduces the experimental results for the monolayer graphene Faraday rotation obtained by Crassee et al. [7] provided that the appropriate Drude-like frequency- and magnetic field-dependent conductivity tensor $\sigma(\omega, B)$ is employed. The expression for the conductivity tensor is equal to that of reference [7] divided by the thickness of the simulated graphene layer to have the physical dimension of a bulk conductivity. It has to be noticed that graphene is the only material that presents an optical non-reciprocal behaviour in this structure. Focusing on the quasi-classical regime of the graphene magneto-optical response [7, 17, 18] – where the splitting of the two Landau levels around the Fermi energy (E_F) is much smaller than E_F itself – the conductivity is well described by the Drude model. This is characterized by the presence of the quasi-classical cyclotron resonance, whose frequency is given by $\omega_c = eBv_F^2/E_F$, with e the electronic charge, B the amplitude of the magnetic field, and v_F the Fermi velocity. For Fermi energies of the order of hundreds of meV and for magnetic fields of a few Tesla, ω_c falls in the THz range. In this classical regime, the elements of σ are functions of the graphene Drude parameters, such as B, E_F, v_F and the scattering time τ. The magnetic field, Fermi velocity and the scattering time were always fixed equal to 7 T, 1.01×10^6 m/s and 8.05×10^{-14} s, respectively, while the Fermi energy is varied in the range between 0.1 and 0.4 eV with step of 0.1 eV corresponding to an electron mobility $\mu = e\tau v_F^2/E_F$ in the range between $\simeq$ 2100 and $\simeq$ 8400 cm^2/V·s. These values are consistent with those observed in magneto-optical experiments on mono-layer graphene ([7, 8]). The graphene sheet is then separated by a 200 nm thick layer of SiO_2 from the 100 nm thick gold metasurface of optical resonators. The role of this insulating layer (with refractive index n $\simeq$ 1.95 and absorption coefficient $\alpha < 10$ cm^{-1} [19]) is to electrically isolate graphene from the underneath gold metasurface. The structure is assumed to be placed on a substrate of infinite thickness in order to avoid the Fabry-Pérot interference which is, for our purposes, a spurious effect. Moreover, even though in a realistic situation the substrate-air interface is always present, the Fabry-Pérot can be mitigated by reducing the substrate thickness to values much smaller than the wavelength or it can be almost totally suppressed by using an antireflection coating.

The simulation domain was defined by unit cell Floquet boundary conditions along the metasurface planar directions, while the vertical stack was enclosed between two perfectly matched layers, one on top of the air super-strate, and one on the bottom of the substrate. As schematized in Fig. 1, we consider the interaction of linearly polarized light propagating

Optics EXPRESS

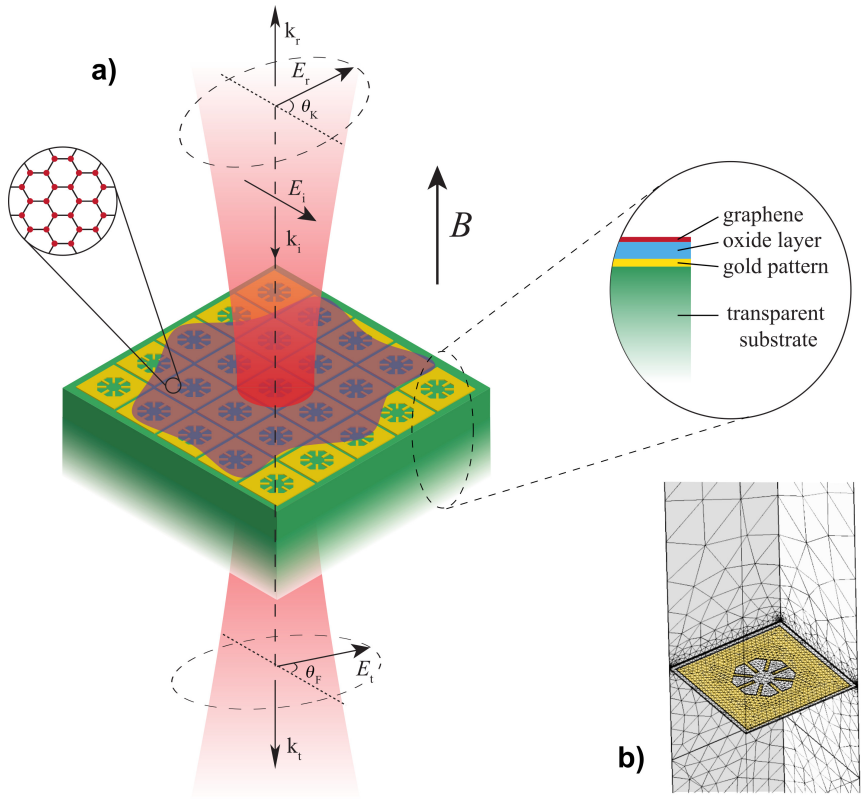

Fig. 1. (a) Device sketch showing the geometry of the simulated structure: a monolayer graphene is separated by a 200 nm thick layer of SiO_2 from the 100 nm thick gold metasurface. This stack is placed above an ideally infinite and transparent substrate. Linearly polarized light with electric field $\mathbf{E}_i$ is incident on the structure. It is transmitted with electric field $\mathbf{E}_t$ rotated of an angle θ_F, i.e. the Faraday angle. The same effect is possible in reflection giving rise to the Kerr rotation with a polarization rotation of an angle θ_K, i.e the Kerr angle. The direction of the magnetic field is parallel to the direction of propagation and its verse points towards the positive z-axis. The magnetically induced circular dichroism of graphene gives rise to a small degree of ellipticity in the polarization of both reflected and transmitted waves. (b) Internal view of the mesh grid of the simulated unit cell. The inset highlights the mesh in the metasurface plane with the resonator in yellow.

perpendicularly to the structure and parallel to the direction of the external magnetic field. Then, we analyze the intensity and state of polarization of both the transmitted and reflected electromagnetic wave. In order to calculate the non-reciprocal rotation angle, two simulations in which light propagates in opposite directions were performed. The non-reciprocal single-pass rotation angle was defined as the mean value between the angles from the two simulations. In our case, these angles were always found to be equal, both in amplitude (at least up to the third decimal place in radiant units) and sign. The latter was considered positive or negative depending whether the polarization was turned counter-clockwise or clockwise, respectively.

In Fig. 1(b) the mesh grid of the simulated unit cell is shown. The three-dimensional space is divided in tetrahedral elements with linear dimension more than five times smaller than the light wavelength in each material. In the metasurface plane the mesh is composed by triangular elements with minimum and maximum size of 0.05 μm and 0.5 μm, respectively, with a maximum element growth rate of 1.01. This resolution of the mesh allows to reproduce correctly

Optics EXPRESS

the electromagnetic response of certain metasurfaces described in the literature [16, 20, 21].

3. Dependence of the performance on the resonator geometry

Our analysis starts from studying the effect of ordinary square electric-split ring resonators (SRRs) [20, 22] on the graphene non-reciprocal properties. Although this simple shape, the presence of the hybrid metasurface induces an increase of the Faraday rotation in correspondence of the SRRs resonance. By optimizing the geometric parameters of the resonator shape, the structure is observed to produce giant Faraday rotation. The geometry, which belongs to the D_2 symmetry group and resulting from the optimization process, is shown in Fig. 2(a), while the simulated Faraday angle θ_F is represented by the red curve in Fig. 2(d) obtained for $E_F = 0.3$ eV and a refractive index of the substrate equal to 1.5. A broad peak (FWHM of $\simeq$ 1.2 THz) of Faraday rotation can be observed, with a maximum angle of $\simeq$ 0.48 rad (more than 27.5°) at $\simeq$ 6.3 THz (Fig. 2(d)). Due to the geometric symmetry, the electromagnetic response of the metallic metasurface is polarization dependent. In fact, we observed that the polarization parallel to the x-axis (Fig. 2(g)) provides a much larger amplification than the perpendicular one ($\mathbf{E} \parallel \hat{y}$). For this reason, in the rest of the manuscript we report the result only for $\mathbf{E} \parallel \hat{x}$. By comparing the maximum value of θ_F obtained with the hybrid metasurface with the maximum one (0.1 rad) achieved with monolayer graphene only [7], we found an amplification of a factor $\simeq$ 4.6. However, as it can be observed from the blue curve in Fig. 2(d), the intensity of the transmitted light in correspondence of the Faraday rotation peak has its minimum, with a value even lower than 1% of the intensity of incoming light.

As the frequency range of the Faraday effect enhancement is achieved in correspondence of the metasurface resonance, the device operating frequency can be easily chosen by rescaling the dimension of the metasurface unit cell. For the chosen values of the metasurface unit cell and single resonator size (see Table 1), the metasurface resonance falls in the THz range.

Unfortunately, this geometry has a very small transmission spectrum that may limit the potential application of the system. Here, in order to exploit the potential of this hybrid metasurface for an efficient non-reciprocal device, a large polarization rotation accompanied by an appropriately high transmittance is highly desiderable. Starting from the observation that the magneto-optical response of the proposed structure depends on the geometric parameters and with the aim to increase the transmission of the system, different geometries for the resonator were considered. Based on the hypothesis of a link between polarization rotation and the symmetry of the metasurface resonator, we analyzed, and optimized, the resonator shapes having different degree of symmetry. A succinct resume of this optimization process is reported in Fig. 2. Starting from the previously mentioned D_2 shape, other geometries with increasing symmetry are investigated. We present two of them, belonging to the D_4 and D_8 symmetry group, in Fig. 2(b) and Fig. 2(c) respectively. More precisely, only the symmetry of the resonator center is increased, while the outer shape remains a square in all geometries. Besides the length of the unit cell (indicated with the letter a in Fig. 2(a)), all the considered geometries are described by the same four parameters showed in Fig. 2(a): the length b of the resonator, the width w of the resonator wire, the length g of the gap and the width p of the gap bearing side. In this way, both D_4 and D_8 shapes were obtained by making the D_2-geometry invariant by rotation around the transversal axis of 90° and 45°, respectively. Interestingly, the center of the resonator is recognized to be the part that mainly contributes to the resonance buildup. In fact, changing the outer shape of the unit resonator, no modifications are found in the magneto-optical response of the system, if the distance between adjacent resonators is not varied. This is a consequence of the confinement of electromagnetic fields almost in the center of the planar geometry, as it can be clearly seen in Fig. 2(g), where the spatial distribution of the e.m. fields close to the metasurface are shown.

As shown in Fig. 2(d), Fig. 2(e) and Fig. 2(f) strong differences in both transmittance T and

Optics EXPRESS

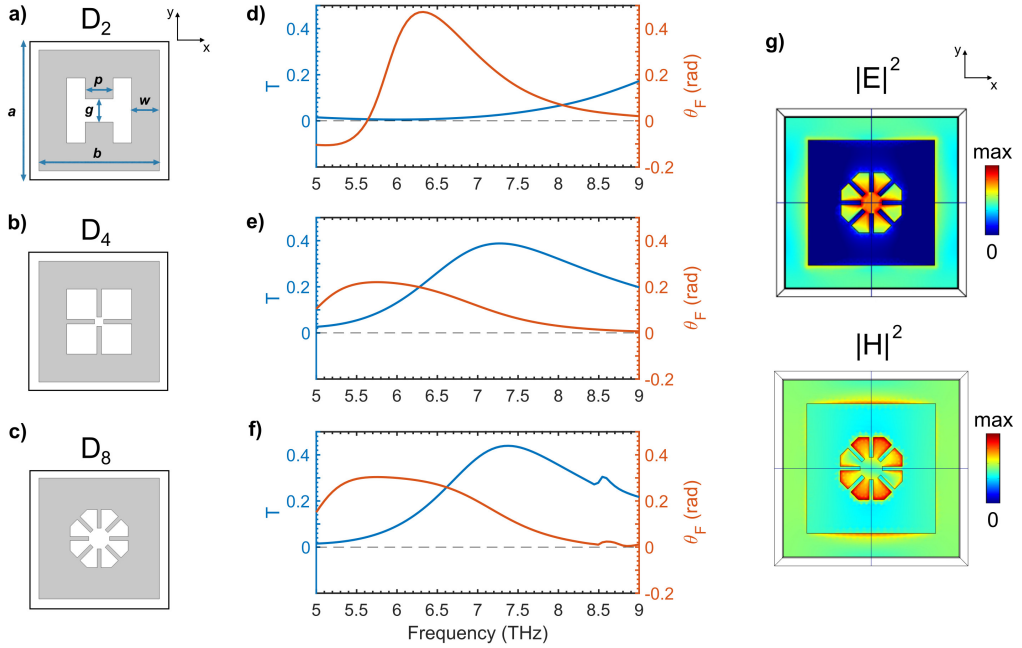

Fig. 2. Panels a-c: Three geometric shapes of the resonators belonging to the D_2, D_4 and D_8 symmetry groups, respectively. Each of them constitutes the unit element of a metasurface arranged in a square array. The unit cell length a and the four parameters that characterize the resonator (b, g, p and w) are indicated in panel (a). Depending on the specific shape, the values of these parameters change in order to optimize the non-reciprocal behaviour of the system. The values of these parameters for each geometry are reported in Table 1. Panels d-f: Transmittance (T, blue curve) and Faraday angle (θ_F, red curve) calculated by FEM simulations in the frequency range between 5 and 9 THz for the structure in Fig. 1 with the shapes of the resonator shown in panels (a), (b) and (c), respectively. The graphene Fermi energy is fixed at 0.3 eV for all the three geometries. The refractive index of the substrate, considered of infinite extension for simplicity, is set to 1.5 in all the simulations, while the external magnetic field is fixed to 7 T, the maximum used in [7]. (g) Spatial distribution in the metasurface plane of the square modulus of the electric ($\mathbf{E}$) and magnetic ($\mathbf{H}$) field of the propagating light at 6.5 THz using a logarithmic color scale. The direction of polarization is always parallel to the x-axis, i.e. $\mathbf{E} \parallel \hat{x}$.

Faraday angle θ_F can be observed in the three different geometries. Even though the maximum Faraday rotation decreases as the symmetry is increased, the enhancement of the Faraday effect is still observed in all three structures, with values for the maximum Faraday angle of $\simeq 0.22$ rad ($\simeq 12.6°$) and $\simeq 0.3$ rad ($\simeq 18°$) for D_4- and D_8-geometry, respectively. However, the most interesting result is the strong dependence of the transmittance on the resonator shape. The metasurface resonance not only shifts in frequency and changes in shape, but it also acquires an increased overall transmittance, though the portion of the surface covered by the gold pattern does not vary significantly by changing the resonator shape. In particular, in the frequency region around the maximum Faraday rotation the transmittance assumes values of more than 20% both in the case of D_4- and D_8-geometry. This is also due to a smoother peak of the Faraday rotation with a progressive increase of its FWHM which reaches $\simeq 2.3$ THz for the geometry belonging to D_8-group. It is worth to note that, thanks to their symmetry, the two geometries in Fig. 2(b) and Fig. 2(c) are characterized by a polarization independent electromagnetic response that makes them more versatile in view of applications compared to less symmetric geometries.

Optics EXPRESS

4. Study of the figure of merit

As described in reference [23] (according to the type of non-reciprocal device, isolator or rotator) it is possible to quantify the compromise between the transmitted (or also reflected) intensity and the polarization rotation by using a specific figure of merit. In the case of Faraday rotation, the intrinsic figure of merit γ_F as a function of the transmittance T and Faraday angle θ_F can be defined as:

$$\gamma_F(T, \theta_F) = \frac{|2T \sin \theta_F|^2}{(1 - T^2)^2} \tag{1}$$

The optimal non-reciprocal performances achievable using any graphene-based design are strictly limited by the graphene conductivity tensor. In fact, γ_F must satisfy the fundamental inequality $\gamma_F \leq \gamma_{NR}$, where γ_{NR} is the graphene non-reciprocal upper bound. The dimensionless factor γ_{NR} is in general a function of both the real and imaginary part of the conductivity tensor, but in the classical regime, it acquires the following simple expression as a function of the graphene Drude parameters v_F, E_F, τ and the magnetic field B:

$$\gamma_{NR} = \left(\frac{Be\tau v_F^2}{E_F} \right)^2 = (\mu B)^2 \tag{2}$$

Therefore, in order to establish the best performance parameters for our system, we compared the figures of merit γ_F for the Faraday effect quantified as a function of θ_F and T. The results are shown in Fig. 3 as a function of frequency. For each metasurface, γ_F is calculated for four values of the Fermi energy (0.1, 0.2, 0.3 and 0.4 eV) and for two different refractive indices of the substrate. Instead, the magnetic field continues to be fixed at $B = 7$ T. The left column, composed by Fig. 3(a), Fig. 3(b) and Fig. 3(c), presents the results in the case of refractive index $n = 1.5$, while the right column shows the ones relative to $n = 2.5$. In order to have approximately the same frequency region for both values of n, the size of the unit cell for $n = 2.5$ is scaled by a factor $\simeq 0.6$, which is equal to the ratio between the two refractive indices; indeed, the frequency of maximum Faraday rotation varies proportionally to n^{-1}. Passing from the panel on the top to the one at the bottom of each column, the geometries are sorted with increasing symmetry, i.e., D_2, D_4 and D_8. The values of the geometric parameters for the three geometries are reported in Table 1.

Table 1. Values of the geometric parameters for the three described shapes belonging to the D_2, D_4 and D_8 symmetry group in the cases of refractive index n equal to 1.5 and 2.5. These values were chosen in order to have approximately the maximum of the figure of merit for $E_F = 0.2$ eV at 6.9 THz.

Group	n	a (μm)	b (μm)	w (μm)	p (μm)	g (μm)
D_2	1.5	17.8	16.6	3.8	3.8	3.2
	2.5	11.2	10.4	2.4	2.4	2
D_4	1.5	16.6	15.4	3.5	0.6	1.2
	2.5	10.2	9.5	2.2	0.4	0.74
D_8	1.5	23.7	22	5.7	0.7	3.8
	2.5	15.2	14.1	3.7	0.4	2.4

Optics EXPRESS

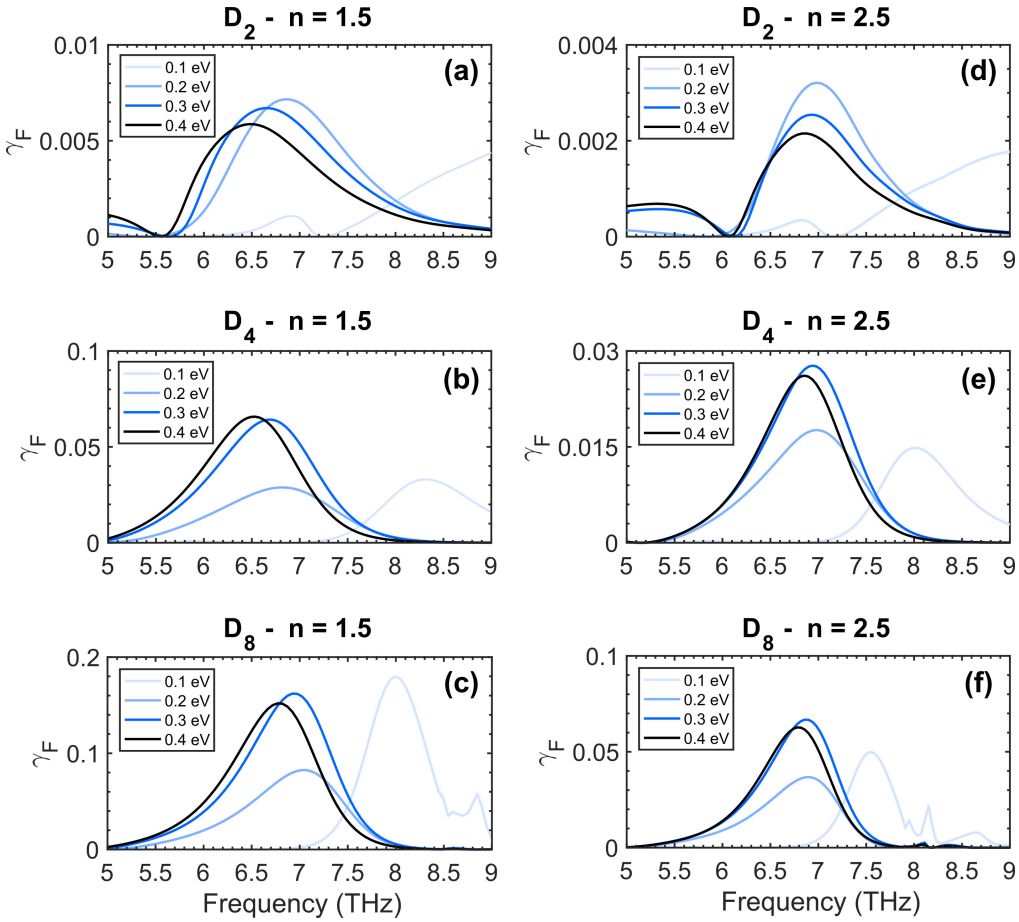

Fig. 3. Calculated values of the figure of merit γ_F for the Faraday effect given in Eq. (1) for the three studied geometries. Panels (a), (b) and (c), i.e. the left column, show the results obtained for a refractive index, n, of the substrate equal to 1.5, while panels (d), (e) and (f), right column, present that for n = 2.5. In each column, the graphs are sorted accordingly to the structure symmetry, passing from D_2 (panels (a) and (d)) to D_4 ((b) and (e)) and then to D_8 ((c) and (f)). In each panel the values of γ_F were obtained for four different Fermi energies (0.1, 0.2, 0.3 and 0.4 eV). The external magnetic field is always fixed at 7T.

First of all, the main observation is the improvement of γ_F when increasing the symmetry of the resonator geometry. For both values of n, the maximum amplitude of γ_F gains almost an order of magnitude when passing from D_2- to D_4-shape. With the D_8-geometry, γ_F makes a smaller improvement, but it is still more than doubled with respect to the value achieved with the D_4-shape. Secondly, comparing the results obtained for the two values of n, we observe a larger figure of merit in the case of lower refractive index for each structure.

Moreover, we found a strong dependence of γ_F on the graphene Fermi energy. Both the peak frequency and the peak value of the maximum of figure of merit change. If we compare the curves resulting from different n, but with the same geometry, γ_F shows almost a very similar behaviour with E_F. For the case of the D_2-shape, the frequencies of maximum γ_F shift when the Fermi energy is varied, but the maxima of γ_F are not monotonic in E_F (the maximum of γ_F is the highest at E_F = 0.2 eV and then it progressively decreases). Going to the more symmetric shapes, nearly the same frequency positions of the maxima are found comparing Fig. 3(b) with Fig. 3(e),

Optics EXPRESS

and Fig. 3(c) with Fig. 3(f). In Fig. 3(b), the maximum for E_F = 0.4 eV is slightly higher than the one at 0.3 eV, while in Fig. 3(e) it is just the opposite. The same also happens to the maxima for E_F = 0.2 and 0.1 eV. Between Fig. 3(c) and Fig. 3(f) for the D_8 geometry, the most evident difference is observed in the curves for E_F = 0.1 eV, for which the maximum γ_F passes from the highest achieved value for n = 1.5 to an intermediate level for n = 2.5.

It is worth to note that, for the case of D_2-shape, the figure of merit peaks where the transmittances are at their minimum. On the contrary, for the D_4- and D_8-shapes, γ_F peaks in a point where the slightly decreasing θ_F and rapidly increasing T meet, whilst being far from their respective minima. This ensures a reasonable choice of both θ_F and T which can be employed in a realistic device. In particular, for the striking case of D_8-geometry, with E_F = 0.1 eV and n = 1.5, the γ_F peak appears at frequencies where the transmittance assumes large values, but where θ_F is relatively small; that is, transmittance of 63% and θ_F of 0.1 rad, respectively. The width of the peaks is instead similar for all the structures. Apart from the curves at E_F = 0.1 eV for any geometries, the FWHM of the γ_F peak are all in the range between 1.2 and 1.4 THz, allowing to maintain good performance in a broad frequency region. The differences, in the frequency position of γ_F maximum and sometimes shape, of the figures of merit for E_F = 0.1 eV with respect to the other doping levels should be ascribed to the E_F-dependence of the graphene Drude conductivity.

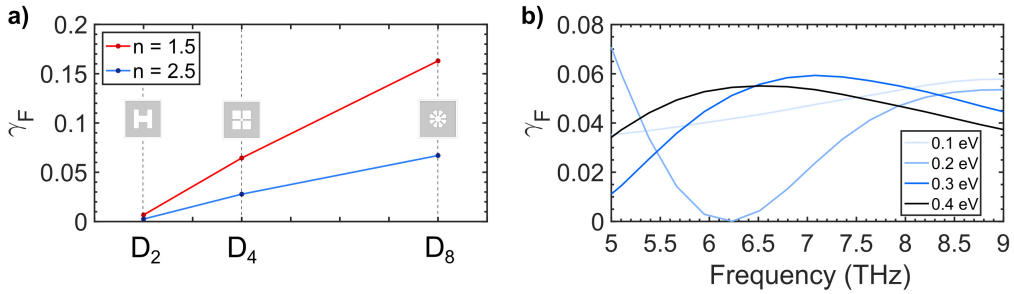

Fig. 4. (a) Evolution of the maximum value assumed by the figure of merit γ_F of the system defined in Eq. (1) as a function of the symmetry group of the resonator shape. The red and blue curves show the results for the refractive index n equal to 1.5 and 2.5, respectively. The three dashed vertical lines indicate the studied symmetry groups, D_2, D_4 and D_8, shown by the three insets. (b) The simulated γ_F for the bare monolayer graphene is shown for comparison in the frequency range of interest.

The evolution of the figure of merit with the symmetry of the chosen resonator shape is summarized in Fig. 4(a). Here, the maximum achieved values of γ_F are plotted for the three described geometries for both the investigated values of n of the substrate and only for E_F = 0.3 eV. From the graph, it is clear that there is a steady improvement of the performance of the system when going from low to high symmetries. Interestingly, this occurs for both values of n. Nevertheless, the figure of merit obtained for the lower refractive index is always larger than that obtained for the higher one. We note that the refractive index n = 1.5 has a technological relevance. Indeed, it is approximatively the refractive index of the cyclic-olefyn copolymer (COC), which is a polymeric substrate commonly employed in the THz range thanks to its low and flat absorption coefficient (< 3 cm^{-1}). As comparison we show in Fig. 4(b) the resulting γ_F for the single-layer graphene in the case of n = 1.5 for various Fermi energies in the same frequency range. Even though the achieved values of γ_F are quite distant from the non-reciprocal upper bound γ_{NR} (equal to $\simeq$ 3.8 in the case of E_F = 0.3 eV), adopting this hybrid metal-graphene metasurface we obtain values of γ_F more than doubled with respect to the case of the bare mono-layer graphene.

Optics EXPRESS

Proceeding to further increase the symmetry of the resonator geometry (passing for example to D_{16}-symmetry), we observe a little enhancement (few %) of the transmission and a small variation of Faraday rotation with respect to the resonator belonging to the D_8-group. However, the small improvement of the figure of merit does not justify the adoption of higher symmetric shapes for practical devices, due to the complication in the fabrication process arising from the increased geometric symmetry. For this reason, the study of resonators with a higher symmetry degree is not reported systematically in the present work.

The results presented so far suggest that the performance of a Faraday rotator consisting in a metal-graphene metasurface are strongly correlated with the degree of symmetry of the metallic resonating element, whose shape was here inspired by a generalization of the electric split ring resonator geometry. Without aiming at getting general conclusions about the role of symmetry applicable to any kind of geometry, we attempt here to answer the question whether the quite restrictive assumption that the resonator belongs to the dihedral group D_n is central to our conclusions. A slightly less general symmetry condition - but actually more properly connected to the rotational properties - is the belonging to the cyclic group C_n: an object belongs to C_n if it can be superimposed to itself upon rotations of $2\pi/n$. Clearly, belonging to D_n implies belonging to C_n, but not vice-versa.

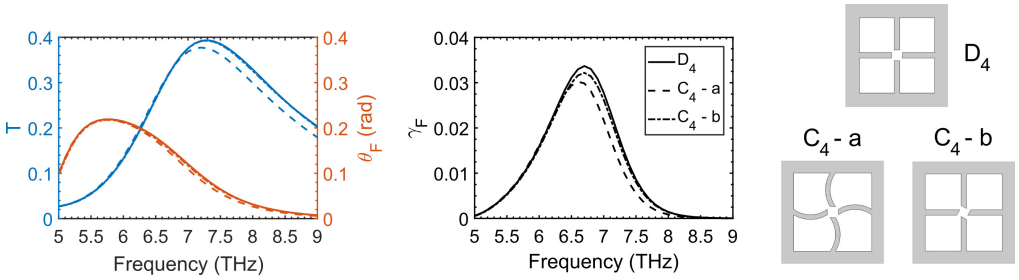

Fig. 5. Transmittance T, Faraday angle θ_F and figure of merit γ_F for three geometries: the D_4-geometry presented in Fig. 2 and two geometries belonging to the C_4 symmetry group, named C_4 - a and C_4 - b. These last structures are obtained from D_4 by modifying the central part of the resonator but maintaining the same values for the geometric parameters defined in Fig. 2.

Figure 5 reports the non-reciprocal optical response of three resonators: one is the D_4 analyzed previously, which is here compared with two resonators belonging to C_4 but not to D_4. The structural parameters were changed either in the shape of the finger (C_4 - a) or in the shape of the finger tip (C_4 - b). Strikingly, all the spectra of interest are only slightly affected by lowering the symmetry passing from the dihedral to the cyclic group, as evident comparing the obtained γ_F.

Far from being exhaustive, this study suggests that a higher grade of cyclic symmetry may be considered as an indicator of good magneto-optic nonreciprocal response, when the resonators are coupled with graphene or with another magneto-optic thin material. These conclusions, which we reached through a process mostly based on numerical experiments, are indeed supported by physical intuition: in order to support resonantly enhanced polarization rotation, a structure must be able to withstand a (transmissive) resonance whose local field can effectively overlap with arbitrary polarization directions. In that way, the fields can appropriately couple in and out at arbitrary directions of the polarization plane.

5. Analysis of the non-reciprocal properties in reflection

Focusing on the properties of the light reflected from the system, we observed that a huge non-reciprocal polarization rotation is possible also in reflection. The simulated Kerr angle θ_K

Optics EXPRESS

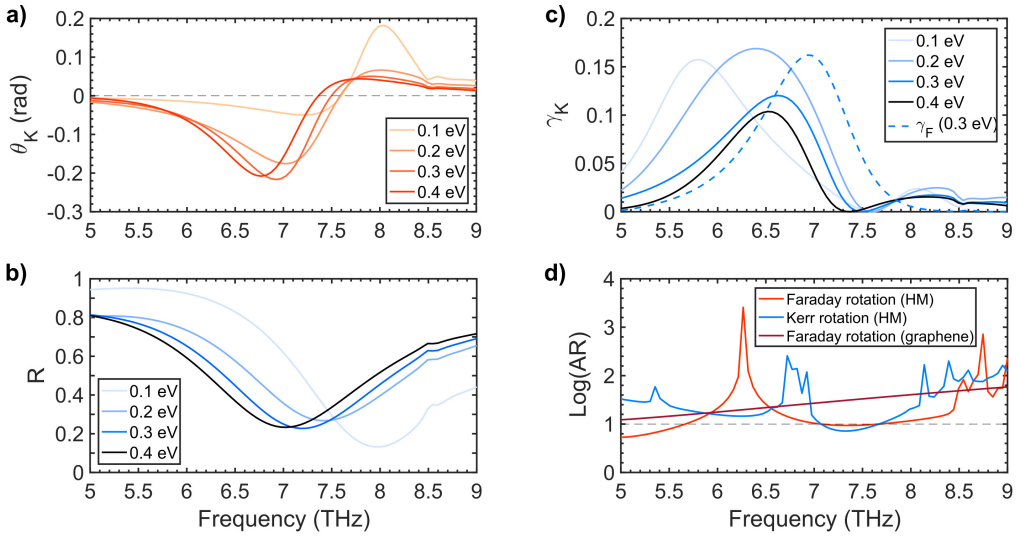

Fig. 6. (a, b) Simulated Kerr angle θ_K and reflectance R for the metasurface with resonator geometry belonging to D_8 symmetry group in the case of refractive index of the substrate equal to 1.5. The curves were obtained for four values of the Fermi energy of graphene E_F = 0.1, 0.2, 0.3 and 0.4 eV. (c) Results for the figure of merit γ_K for the Kerr effect obtained from the values of θ_K and R presented in panel a and b. As a comparison, the dashed curve represents γ_F for the same geometry at E_F = 0.3 eV. (d) Axial ratio (AR) obtained for both the Faraday rotation (red curve) and Kerr rotation (blue curve) in the case of E_F = 0.3 eV for the hybrid metasurface (HM). The brown curve represents the simulated AR for the Faraday effect of monolayer graphene. The external magnetic field is fixed at 7T.

and reflectance R are shown in Fig. 6(a) and Fig. 6(b), respectively, for the four values of E_F already considered in the transmission study. Here, the sign of the polarization rotation is in the opposite direction with respect to the Faraday rotation, but similar features, frequency shifts and shape variations of the resonance peak as a function of the Fermi energy are still present. The maximum negative value for θ_K of $\simeq$ -0.22 rad is achieved for E_F = 0.3 eV at approximatively 6.9 THz with a reflectance of $\simeq$ 22% (Fig. 6(a) and Fig. 6(b)). The figure of merit γ_K for the Kerr effect (defined as γ_F in Eq. (1), but replacing θ_F and T with θ_K and R, respectively) is reported in Fig. 6(c). As for the Faraday effect, the γ_K peak for E_F = 0.1 eV arises from a huge reflectance (> 95%) and a moderate polarization rotation, $\theta_K < -0.01$ rad. The most interesting curve is instead obtained for E_F = 0.2 eV. It presents the highest maximum value for γ_K of $\simeq$ 0.17 with a FWHM of $\simeq$ 1.5 THz. It is also interesting to compare this curve with that obtained for the Faraday effect at E_F = 0.3 eV, represented with dashed line, which shows the maximum value for γ_F. We can observe that the frequency band of operation of the system, depending whether it is working in transmission or reflection, is different; at E_F = 0.3 eV, the maxima of the figure of merit occur at $\simeq$ 6.5 THz and 7 THz in the case of reflection or transmission, respectively.

A crucial property to be considered is the ellipticity of the radiation. Even though the magnetically induced circular dichroism of graphene is an unavoidable effect, a device would take great advantage of an almost purely linear polarization state. Thus, we considered the ratio between the major and the minor axis of the polarization ellipse, i.e. the axial ratio (AR), for both transmitted and reflected wave. In Fig. 6(d) (in the case of E_F = 0.3 eV), we report the logarithm of AR for the hybrid metasurface as red and blue curves calculated for the Faraday and Kerr configurations, respectively. It can be observed that in the whole studied frequency region the AR remains above or very near to 10. This value is very similar to the one derived in monolayer

Optics EXPRESS

graphene, here reported for comparison as a brown curve.

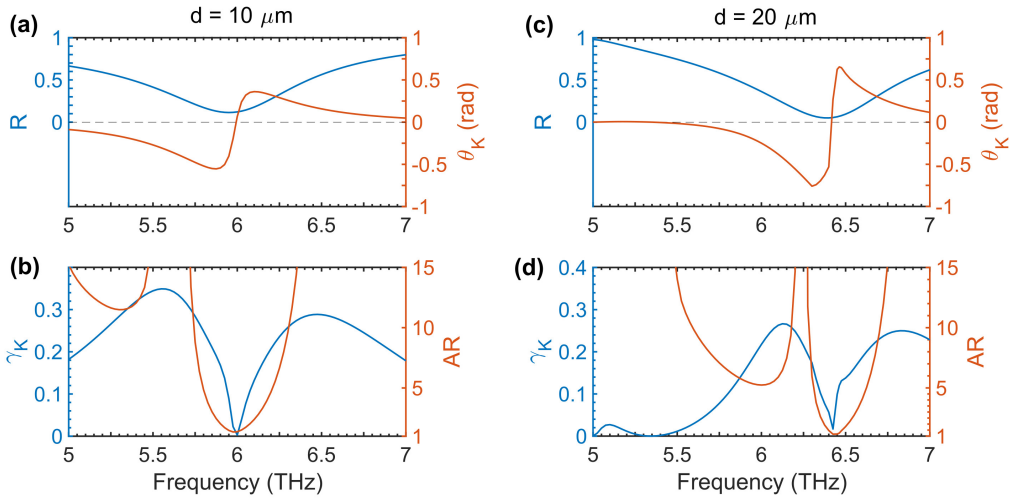

Fig. 7. Results for the system with the D_8 metasurface geometry allowed to work only in reflection by the presence of a 50 nm thick gold layer at the bottom of the structure shown in Fig. 1. Simulations are performed for two different values of thickness d of the substrate with refractive index $n = 1.5$ in the frequency range from 5 to 7 THz. In the left column, panels (a) and (b), the reflectance (R), Kerr angle (θ_K), the corresponding figure of merit (γ_K) and the axial ratio (AR) are shown for $d = 10$ μm. In the right column, panels (c) and (d), the same quantities are reported for $d = 20$ μm. The graphene Fermi energy is set to 0.3 eV.

Finally, we studied the system in a reflection-only configuration. By adding a 50 nm gold uniform layer below the substrate, the transmission through the structure is prevented; the incident light intensity is totally distributed in reflection and absorption. As previously, we calculated the values of the reflectance R, Kerr angle θ_K, figure of merit γ_K and axial ratio AR in the frequency range from 5 to 7 THz for $E_F = 0.3$ eV. For the D_8 symmetry resonator these quantities are obtained for different values of thickness (d) of the substrate with $n = 1.5$. In order to show the major consequences implied by the choice of d, we report the results for two values of d (10 μm and 20 μm) in Fig. 7. The results for $d = 10$ μm are shown in Fig. 7(a) and Fig. 7(b), while those for $d = 20$ μm are presented in Fig. 7(c) and Fig. 7(d). In both cases, we observe not only a further enhancement of the non-reciprocal polarization rotation, but also an increase of the figure of merit with respect to the configuration without the gold layer underneath. The amplification of the Kerr rotation appears at different frequencies depending on the substrate thickness due to a shift in the metasurface resonance. The curves for the Kerr angle present a similar resonant feature characterized by two peaks, one negative at lower frequencies and one positive at higher frequencies. For both thicknesses, the absolute value of Kerr rotation is higher for the negative peak. The maximum achieved θ_K are $\approx$ -0.55 rad ($\simeq 32°$) with $AR \simeq 3$ at $\simeq 5.9$ THz and $\simeq$ -0.76 rad ($\simeq 43.5°$) with AR bigger than 10 at $\simeq 6.3$ THz for $d = 10$ μm and $d = 20$ μm, respectively. Despite the quasi-optimal polarization rotation for the larger value of d, the configuration with $d = 10$ μm presents a maximum $\gamma_K \simeq 0.35$ at 5.55 THz, a factor $\simeq 1.3$ with respect to the maximum γ_K ($\simeq 0.27$) at 6.1 THz in the case of $d = 20$ μm. It is interesting to note that for both thicknesses at the frequency of zero Kerr angle, corresponding also to the zero in γ_K, the polarization is approximatively circular ($AR \approx 1$). At the sides of this frequency, two broad peaks appear. For $d = 10$ μm, these peaks have a FWHM of about 1 THz. In particular, the region around 5.5 THz and the one around 6.5 THz represent the best regions for the system

Optics EXPRESS

operation due to the *AR* much larger than 15, yielding to a system that operates as Kerr rotator preserving almost linear polarization.

6. Conclusions and perspectives

In conclusion, in this work we showed by full wave simulations that a metasurface, whose resonant elements are metallic patterns with an unconventional geometry, can significantly enhance the non-reciprocal response of monolayer graphene. This hybrid metal-graphene metasurface provides a strong amplification of both the Faraday and Kerr effect with respect to monolayer graphene over a broad range of THz frequencies, still preserving a high transmittance or reflectance, respectively. The main result of the article is that this enhancement of figure of merit of the system, i.e. the factor defined in Eq. (1) which describes the performance as a compromise between the transmission (or reflection) intensity and the amount of non-reciprocal polarization rotation, is induced by increasing the geometric symmetry of the resonators constituting the metasurface. Passing from a resonator shape belonging to the D_2 symmetry group to one of the D_8 group, a factor of more than an order of magnitude is gained and a factor of about 2.7 with respect to the figure of merit for the Faraday rotation in monolayer graphene at the same frequencies. In particular, the maximum achievable Faraday rotation ($\theta_F \simeq 18°$) is triple and double in amplitude with respect to the maximum achieved Faraday angle with the bare monolayer graphene ($\theta_F \simeq 6°$ [7]) and single-layer graphene exploiting a FP-cavity ($\theta_F \simeq 9°$ [9]).

The relevance of other parameters of the structure, like the Fermi energy of graphene and the refractive index of the substrate, was also investigated. The graphene Fermi energy is seen to strongly affect the non-reciprocal properties, changing both the frequency range of operation and the maximum value of the figure of merit. We have to highlight that the patterned metal has a multifunctional role. Beyond its exploitation as resonant metasurface, it could be used to apply a voltage gate: if the metallic metasurface is arranged in a connected fashion, the graphene Fermi energy could then be varied allowing to tune the system to the desired frequency range of operation. The study of the refractive index of the substrate revealed that a lower value of n is recommended for a better performance of the system.

Furthermore, by considering a configuration of the system able to work only in reflection we obtained values of the figure of merit even larger. Depending on the thickness of the substrate it is possible to obtain different performances; the achievement of up to 43° of Kerr rotation with a figure of merit $\simeq 0.27$ or lower rotation angle ($\simeq 32°$), but with a figure of merit up to 0.35 (a factor $\simeq 2.2$ with respect to the previous configuration working both in reflection and transmission).

As a future development, we can consider the use of boron nitride-graphene-boron nitride stack to further enhance the performance of the hybrid non-reciprocal metasurface thanks to the fundamental connection between the mobility and the performance of the non-reciprocal system, Eq. (2). In our work, this crucial parameter is varied in the range between $\simeq 2100$ and $\simeq 8.400$ $cm^2/V{\cdot}s$ depending on the choice of the Fermi energy. With the adoption of advanced materials, such as graphene embedded in two boron nitride-sheets, the graphene mobility can reach values $\simeq 40.000$ $cm^2/V{\cdot}s$ [24], paving the way to practical devices.

Funding

European Union Seventh Framework Programme (604391); Graphene Flagship and by the European Research Council through the Advanced Grant No. 321122 SouLMan.